Diffuse charge and Faradaic reactions in porous electrodes

P.M. Biesheuvel,[1,2] Yeqing Fu[3] and Martin Z. Bazant[3,4]

[1]*Department of Environmental Technology, Wageningen University, Bornse Weilanden 9, 6708 WG Wageningen, The Netherlands.*

[2]*Wetsus, centre of excellence for sustainable water technology, Agora 1, 8900 CC Leeuwarden, The Netherlands.*

[3]*Department of Chemical Engineering and* [4]*Department of Mathematics, Massachusetts Institute of Technology, Cambridge, MA 02139, USA.*

Abstract

Porous electrodes are widely used in electrochemical systems instead of flat electrodes to boost storage capacities for ions and electrons, to improve the transport of mass and charge, and to enhance reaction rates. Existing porous electrode theories make a number of simplifying assumptions: (i) The charge-transfer rate is assumed to depend only on the local electrostatic potential difference between the electrode matrix and the pore solution, without considering the structure of the double layer formed in between; (ii) the charge transfer rate is generally equated to the salt transfer rate, not only at the nanoscale of the matrix/pore interface, but also at the macroscopic scale of transport through the electrode pores. In this work, we extend porous electrode theory by including the generalized Frumkin-Butler-Volmer model of Faradaic reaction kinetics, which postulates charge transfer across the molecular Stern layer located in between the electron-conducting matrix phase and the plane of closest-approach for the ions in the diffuse part of the double layer. This is an elegant and purely local description of the charge transfer rate, which self-consistently determines the surface charge and does not require consideration of reference electrodes or comparison with a global equilibrium. For the description of the double layer we consider the two natural limits: (i) the classical Gouy-Chapman-Stern model for thin double layers compared to the macroscopic pore dimensions, e.g. for high-porosity metallic foams (macropores >50 nm), and (ii) a "modified Donnan model" for strongly overlapping double layers, e.g. for porous activated carbon particles (micropores < 2 nm). Our theory is valid for electrolytes where both ions are mobile and accounts for voltage and concentration differences, not only on the macroscopic scale of the full electrode but also on the local scale of the double layer. The model is simple enough to allow us to derive analytical approximations for the steady state and early transients. We also present numerical solutions to validate the analysis and illustrate the evolution of ion densities, pore potential, surface charge, and reaction rates in response to an applied voltage.

I. INTRODUCTION

Porous electrodes are found throughout electrochemistry and are often favored over flat electrodes for many reasons [1-4]. For instance, when a gas phase, an electrolyte phase, a catalyst phase and a conductor must be brought together in intimate contact, as in most fuel cells and rechargeable batteries, only a porous structure can possibly fulfill this challenging requirement. When only a liquid or a gas phase contacts the electrode, porous electrodes are used to increase the surface area for

charge transfer, thereby reducing the electrode overpotential (or interfacial resistance), as in fuel cell applications [5,6]. Porous electrodes are also used to increased the charge storage capacity of capacitive electrochemical cells, such as double-layer supercapacitors, which store electrons [7-11], capacitive deionization cells which store ions for water desalination [2,12-24], and capacitive energy-harvesting cells, which exploit the reverse process to extract energy by contacting electrodes alternatingly with water of low and high ionic strengths [25-29].
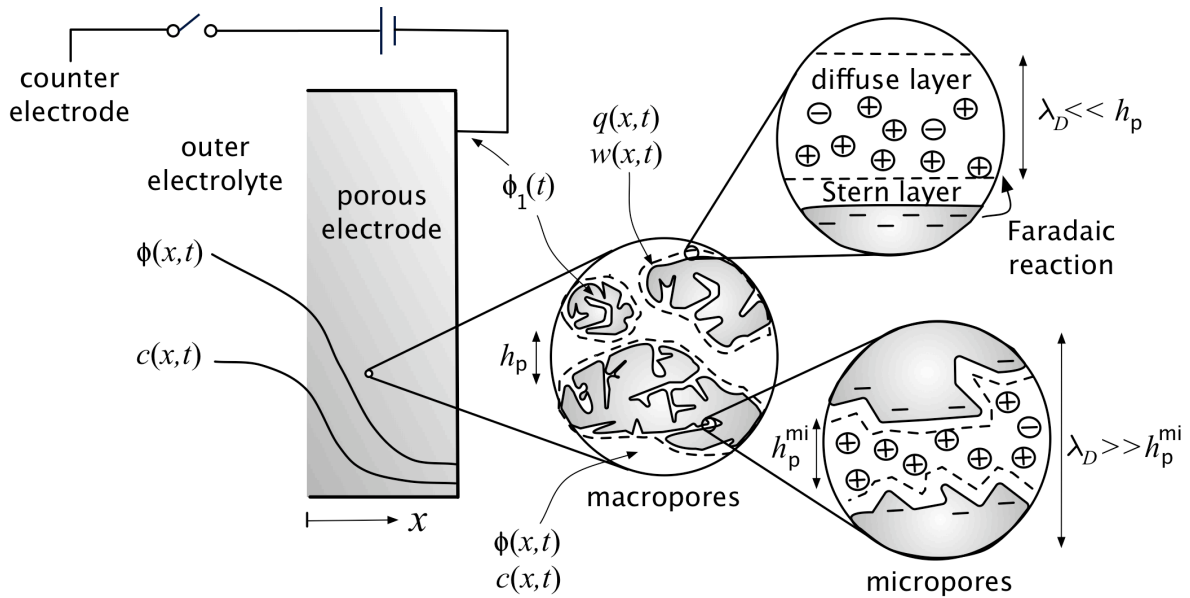

Fig. 1. Schematic representation of our porous electrode theory, which describes ion transport, diffuse charge, and Faradaic reactions across a hierarchy of three length scales: (i) the macroscopic continuum (left) where the volume-averaged variables, such as the bulk concentration $c(x,t)$ and electrostatic potential $\phi(x,t)$, are defined; (ii) the "macropores" (middle) in the pore/particle interphase with thin double layers (dashed lines), whose extent λ_D (the Debye screening length) is much smaller than the mean pore thickness h_p, and which are characterized by their mean charge density $q(x,t)$ and excess salt concentration $w(x,t)$ per area; and (iii) the nano-scale diffuse-charge distribution (right), separated from the electron-conducting phase by a molecular Stern layer (dashed lines) across which Faradaic electron-transfer reactions occur, and occurring either in thin double layers in the macropores (upper right) or in charged "micropores" of thickness $h_p^{mi} \ll \lambda_D$ with strongly overlapping double layers (lower right).

Classical porous electrode theories couple ion transport in the electrolyte phase to either double-layer charging [2,24] or Faradaic charge-transfer reactions [1,3,4], but electrochemical technologies are increasingly involving both processes at the same time. Faradaic reactions are the defining feature of all electrochemical cells, and they can also play an important role in capacitive cells. In desalination and energy harvesting applications, parasitic Faradaic reactions can diminish the efficiency of the process and thus must be understood and quantified. In capacitive energy storage, Faradaic reactions can have a beneficial effect, boosting the energy density of the porous electrode by combining surface-based double-layer capacitance (storing electrostatic energy) with volume-based "pseudo-capacitance" from Faradaic reaction products (storing chemical energy) [7,28,30,31]. These gains in energy density, however, come at the expense of losses in power density, and a general mathematical model would help to tailor this delicate balance for specific applications.

In this work we develop a modified porous electrode theory that simultaneously describes diffuse double-layer charge and Faradaic reactions. The equations are highly nonlinear and contain multiple length and time scales, due to the different physical effects involved, ranging from macroscopic ion transport to nanoscale effects of diffuse charge on charge-transfer reactions, see Fig. 1. We present analytical and numerical results for both steady state conduction (e.g. relevant for fuel cells) and transient charging dynamics (e.g. relevant for capacitive deionization or energy storage, as well as impedance spectroscopy measurements). For simplicity, we focus on relatively dilute aqueous electrolytes, allowing us to neglect ion volume (steric) effects and other non-idealities. To illustrate the approach, we focus here on the simplest case of a Faradaic reaction where the product species is neutral and at fixed chemical potential, as for a metal ion plating out of solution. Extensions can be made to include the fact that the product species must diffuse away as for redox flow batteries, or is intercalated in a host solid compound, where its chemical potential increases, making it progressively more difficult for the reduction to proceed, as for batteries and pseudocapacitors.

The basic assumptions of our model are as follows. We consider a symmetric binary electrolyte with a reactive cation and an inert anion, each monovalent. In steady state (in the absence of convection), the fluxes of the inert ions vanish, and they remain in Boltzmann equilibrium in the mean electrostatic potential. Since the product species is neutral, the current is carried only by the reactive ion in the electrolyte phase, both within the pores of the electrode, and in solution. In this situation, the flux of the reactive ion directly corresponds to the electron current in the external circuit, which significantly simplifies the mathematical description. We stress, however, that in all dynamic processes involving electrolytes, all ions play a part in carrying the current, and we need to include in the model the physical mechanisms that determine the contributions of the various ions to the current at different positions and at different times. As we will show, the key element in this respect is consideration of the structure of the electrostatic double layer (EDL) that forms at the matrix/pore interface within the structure of the porous electrode. Taking for example the classical Helmholtz model where a dielectric capacity (representing solvent molecules on the surface) separates the electrode from the plane containing the countercharge, then counterions are the only species compensating the electron charge. However, due to their thermal motion, ions are not confined into a single plane, but instead diffuse countercharge is distributed in a thin ion cloud next to the interface for which the equilibrium structure is described by the Boltzmann distribution (for ions as point charges). For a planar, semi-infinite dilute electrolyte volume, this "diffuse layer" (or "diffuse part of the double layer") is described by the Gouy-Chapman model. Including a dielectric layer in between the diffuse layer and the charged surface to model a "Stern layer" (or "compact part of the double layer") results in the Gouy-Chapman-Stern (GCS) model for the double layer. The GCS-model can be used in the limit that the Debye length (a measure of the extension of the diffuse part of the double layer) is small compared to the typical pore size. Examples would be electrodes made of conductive metallic foams or close-packed structures of metallic wires, with pore sizes typically above 1 μm.

In many cases, it is important to describe the possibility that the EDLs overlap within a finite pore thickness comparable to the Debye length, as in the case of nano-scale cylindrical or slit-like pores [29,32]. In the limit that the EDLs overlap strongly, i.e. the limit that the Debye length is much larger

than the typical pore size, it is possible to assume a constant electrostatic potential in the pore space. This is the Donnan approach, generally used to describe the ion concentration in homogeneously charged structures such as gels and membranes. In the present work we will make use of a "modified Donnan (mD) model" in which compared to the classical Donnan approach [33,34] two modifications are made: first, a Stern layer is included in between the ionic charge and the electron charge, and second, we include that there is a small non-electrostatic attractive potential, μ_{att}, for the ion to go from the macropores located in between particles (transport pathways) into the micropores of porous particles [35]. This term, μ_{att}, is required to describe data for charge and salt adsorption in porous electrodes as function of applied cell voltage and ionic strength [35]. This model can also be viewed as the simplest limit of more sophisticated double layer models, which capture specific ion-surface interactions and density oscillations induced by ion-ion correlation effects by introducing a suitable external potential near the surface [36,37,38]. That ions have a non-electrostatic attraction into microporous materials such as activated carbons is supported by the fact that these materials absorb salt even without applying a voltage. In the present work we will use the same value of μ_{att} for both ions, but in general they will be different, also differing between different cations, which can be a method to model observed differences in cation adsorption in porous carbon materials [40]. An interesting further difference between porous electrode theory using the GCS-model or the mD-model is that when the GCS-model is used only one type of macroporosity is considered, p, where the anion and cation concentration are the same, with the EDLs modeled as excess surface adsorptions onto a (volumetrically distributed) area, while using the mD-model there are two porosities to consider in the porous electrode theory: the macroporosity p_{mA} (similar to p in the GCS-model), and the microporosity, p_{mi} [39]. In the micropores cation and anion concentration can be different, as we will describe using the mD-model, leading to charge and ion storage. Both the macro- and microphase have locally a mean potential, differing from one another by the Donnan potential, $\Delta\phi_d$.

Compared with the Helmholtz model, both in the GCS- and the mD-model, charge is screened not only by the adsorption of counterions but also by the expulsion of co-ions. In dynamical situations, the normal current into the EDL thus has two independent contributions, both from counterions and from co-ions. The relative contribution of each ion is determined by the choice of EDL model. Note that although we will make use of the GCS- and mD-models in this work, the general framework as we will present can also be applied using other more complicated models for the double layer, e.g. those considering partial double layer overlap, ion volume effects [38,41,42,43], or ion-ion correlations [44].

The structure of this manuscript is as follows. In section II we present our porous electrode-theory including Faradaic charge transfer and derive a simple, dimensionless formulation. In section III we analyze the early-time dynamics and the steady state in response to a suddenly applied voltage between the electrode and the bulk solution. In section IV numerical results are presented to illustrate the predictions of the theory and to test our analytical results for the transient and steady-state profiles of salt concentration, electrical potential, charge density, and Faradaic current. The main text of this paper uses the GCS-model, while the mD-model is derived and applied in Appendix A.

II. THEORY

In this section we describe the porous electrode-theory, which includes ion transport both within the pores of the electrode and within the solution phase outside the electrode, as well as charge formation at the matrix/pore-interface (i.e., at the internal electrode surface), and Faradaic charge transfer there. We only describe the cathode and assume that only cations react faradaically within the electrode. We only consider transport in one dimension across a planar electrode, which is in contact with free solution on one side (x=0) and is blocking for electrolyte and ions on the other side (x=1).

In a full calculation of an electrochemical or capacitive cell the complete solution phase must be considered, including possible in- and outflow of solution into the cell [35,45,46,47]. Here, to simplify matters and to focus on the problem of the electrode, we only describe ion transport toward the electrode through a thin planar layer in front of the electrode, going by various names in the literature, such as the "advection-diffusion layer", "Nernst layer", "(stagnant) diffusion layer", or "mass transfer film". We will use the term "stagnant diffusion layer" and the abbreviation SDL. The thickness of the SDL depends on the extent of turbulence and mixing in the bulk solution [46,48,49]. The SDL is obviously a theoretical simplification of the full problem of diffusion and dispersion of ions in the solution phase, but the concept of an SDL has proven very useful in various problems, e.g., in the field of ion-exchange membranes [50,51] and electrodialysis [45,46,49]. Following ref. [24] we will use a generalized SDL-description (Eq. 4 below), which not only describes the steady state as do the classical expressions for the SDL [46,48,49] but is generally applicable for transient situations. Furthermore, for the situation that the electrolyte is motionless, i.e., not flowing through the cell, this generalized SDL-model is an appropriate description for the full electrolyte space between two (porous) electrodes. For a symmetric system, Eq. 4 can be used with $\partial^2 c/\partial x^2$=0 at the midplane between two symmetric electrodes.

Additional assumptions are that we only consider a 1:1 salt (like NaCl) and assume the diffusion coefficient of the anion and cation in solution, D, to be equal. Within the electrode the diffusion coefficients, D_e, will be lower than in solution, but again we take the same value for the an- and cation. The equations can be easily generalized to describe the case of different diffusion coefficients [45]. We neglect surface conductance, i.e., the enhanced ion transport in the diffuse part of the double layer along a charged interface. Within the solution phase and within the bulk phase of the pores in the electrode we assume local electroneutrality, thus the concentration of cations equals that of the anions, which is the local salt concentration, c. Assuming a much lower resistance for the electrons in the matrix phase than for the ions in solution, we can consider the matrix phase potential, ϕ_1, to be constant, i.e., $\partial\phi_1/\partial x$=0. Important parts of the general theory are similar to material in the theory-section of [24], where a purely capacitive cell was considered without Faradaic charge transfer.

A. Ion transport in the quasi-neutral bulk electrolyte

Within both the stagnant diffusion layer (SDL) and the pores of the electrode (both phases have locally equal concentrations of anions and cations), we assume that the ions are ideal point-charges, so that we can use the Nernst-Planck (NP) equation to describe the ion flux as function of both a

concentration gradient and a migration term due to the electrical field. For the pore solution, the NP-equation can be written in dimensionless form as

$$j_i = -\frac{1}{2}\left(\frac{\partial c_i}{\partial x} + z_i c_i \frac{\partial \phi}{\partial x}\right) \tag{1}$$

where c_i is the dimensionless ion concentration, $c_i = C_i/C_\infty$, of cations or anions (i=+,-), where C_∞ is the constant ionic strength of the bulk solution outside the SDL, and ϕ is the dimensionless electrostatic potential scaled to the thermal voltage, $V_T = k_B T/e$. The dimensionless position coordinate, x, is given by $x = X/L_e$ with L_e the thickness of the electrode. In Eq. (1) the reduced ion flux j_i is given by $j_i = J_i/J_{lim}$ with the diffusion-limited current given by $J_{lim} = 2 \cdot D_e \cdot C_\infty / L_e$.

Based on $i = j_+ - j_-$ and $c = c^+ = c^-$, the ion current, i, follows directly from Eq. (1) as

$$i = -c\frac{\partial \phi}{\partial x}. \tag{2}$$

Eqs. (1) and (2) are valid for the pore space (i.e., we define currents based on the open pore fraction), while to make them valid in solution phase (i.e., in the SDL) the right-hand side in both equations needs to be multiplied by a factor $d_{sdl} = D/D_e$.

Outside the electrode, in the SDL, for each ion a local mass balance can be set up which is given by

$$\frac{\partial c_i}{\partial t} = -2\frac{\partial j_i}{\partial x} \tag{3}$$

where dimensionless time t relates to time τ according to $t = \tau \cdot D_e / L_e^2$. Because we have at each position $c^+ = c^-$, we can sum Eq. (3) and implement Eq. (1) for the two ions to obtain in the SDL

$$\frac{\partial c}{\partial t} = d_{sdl}\frac{\partial^2 c}{\partial x^2} \tag{4}$$

where c without subscript is the local, time-dependent, salt concentration $c = c^+ = c^-$.

At the macroscopic solution/electrode-interface (i.e., at the outside of the electrode, where $x=0$) the following boundary conditions apply. Because the electrode is not fully accessible to the aqueous solution and the ions, a correction because of the porosity, p, must be included, because concentrations, currents, etc., within the electrode are based on the open pore volume. At the interface between solution (the SDL) and the electrode we have continuity in concentration: $c_{sdl} = c_e = c_0$ and potential, $\phi_{sdl} = \phi_e = \phi_0$. The current i on either side is the same but for the porosity correction, thus $i_{sdl} = p \cdot i_e$. Similarly we have continuity in salt flux, thus $d_{sdl}\left.\frac{\partial c}{\partial x}\right|_{sdl} = p\left.\frac{\partial c}{\partial x}\right|_e$. These are the four boundary conditions that apply at the solution/electrode-interface. At the outer boundary of the SDL (at its edge with the bulk solution), we have in the present calculation $c=1$ and $\phi=0$, while at the inner boundary of the electrode (where $x=1$), which we assume to be blocking for all ions, we have $\frac{\partial c}{\partial x} = 0$ and $i=0$.

Different boundary conditions are also possible at the outer edge of the SDL, e.g., $\partial^2 c/\partial x^2 = 0$ for the case of two symmetric and oppositely placed electrodes in a motionless electrolyte, while also a dynamic model can be used where c at the edge of the SDL is a function of time, e.g. because of salt adsorption into the electrodes [51].

Within the electrode, the diffusion equation, Eq. (4), must be modified to include the rate of salt adsorption, j_{salt} (=J_{salt}/J^* where J^*=$J_{lim} \cdot \lambda_D^0 /L_e$), into the double layers at the matrix/pore-interface. Eq. (4) then becomes

$$\frac{\partial c}{\partial t} = \frac{\partial^2 c}{\partial x^2} - \epsilon \, j_{salt} \qquad (5)$$

where the parameter ϵ is the ratio of Debye length λ_D^0 over the characteristic pore thickness, h_p, i.e., $\epsilon = \lambda_D^0 /h_p$. The Debye length $\lambda_D^0 = \kappa^{-1}$ relates to the ionic strength of the bulk solution C_∞ (in mM) according to $\kappa^2 = 8\pi\lambda_B N_{av} C_\infty$, where λ_B is the Bjerrum length, which at room temperature in water is $\lambda_B \sim 0.72$ nm. The effective pore thickness h_p is defined as the ratio of the pore volume to the pore surface area, and is given by $h_p = p/a$, where a is a specific surface area, or pore surface area per total electrode volume, which has units of inverse length [24]. Thus, Eq. (5) describes the variation of concentration c with depth x in the electrode (axial direction), whereas j_{salt} describes how at each position salt is removed from the pores and either adsorbed in the double layer on the electrode surface or consumed by Faradaic reactions. Finally, a local charge balance describes how the (axial) ion current i decreases with depth due to charge transfer to the double layers at the matrix/pore-interface,

$$\frac{\partial i}{\partial x} = -\epsilon \, j_{charge} \qquad (6)$$

where j_{charge}=J_{charge}/J^* describes the charge transfer rate from pore solution into the interface. This finalizes the macroscopic description of transport in the axial macroscopic direction through the pores of the electrodes.

At this point the reader might already wonder how j_{salt} and j_{charge} are calculated, because so far (and throughout the theory section below), at no point is an explicit equation given for either of the microscopic fluxes j directed from macropore into the EDL. There is no inconsistency, however, since these fluxes are implicitly defined by the full set of model equations. Since we assume that at each point in the electrode the EDL is in quasi-equilibrium with local the concentration and potential in the macropore, the microscopic fluxes j are slaved to the local quantities c, ϕ, $\Delta\phi_D$ and $\Delta\phi_S$ (thus also to w and q). The completeness of the model becomes explicit below in section D where the microscopic flux variables are eliminated in a more compact mathematical formulation of the model.

B. Diffuse charge in the double layers

Next we apply the Gouy-Chapman-Stern (GCS) model to describe the double layer formed at the internal electrode area (which is solved at each position x in the electrode) to calculate j_{salt} and j_{charge}. The GCS-model assumes that the double layer is locally flat and thin (compared to the internal length scales of the pores) and remains in quasi-equilibrium, in spite of the passage of normal ionic current, which is valid for thin double layers as long as the current is not large enough to significantly deplete the local bulk salt concentration. For a detailed mathematical justification of the model in the present situation of electrodes sustaining Faradaic reactions, see [52,53]. Similar analyses of the quasi-equilibrium approximation have also been done for transient currents to non-reacting metal electrodes

[54,55] and steady currents to ion exchange membranes [56]. In all of these cases, the GCS model of the double layer emerges as the leading-order approximation of the full Poisson-Nernst-Planck equations describing diffuse charge in a dilute electrolyte in the asymptotic limit of thin double layers $\int \to 0$. In Appendix A we explain and use the modified-Donnan model for the structure of the EDL, valid in the opposite limit, namely of strongly overlapped double layers.

The GCS-model distinguishes between a potential across the Stern layer, $\Delta\phi_S$, and a potential across the diffuse layer, $\Delta\phi_D$, which together compensate the potential difference between the electrode matrix, ϕ_1, and the pore solution, ϕ; thus,

$$\Delta\phi = \phi_1 - \phi = \Delta\phi_D + \Delta\phi_S . \tag{7}$$

This simple equation is an essential element of the model, expressing how the potential in the macropores, ϕ, is directly linked to the potential in the electron-conducting matrix phase, ϕ_1, at the same location and time via the local voltage drop across the EDL, which is in turn related to the local charge density and Faradaic reaction rate through the interfacial model. In particular, the GCS-model is described by three equations: (i) the diffuse-layer charge-voltage relation,

$$q = -2\sqrt{c} \sinh \tfrac{1}{2}\Delta\phi_D \tag{8}$$

where q is a dimensionless surface charge density of the diffuse part of the double layer (multiply by $2, \lambda_D^0$, and C_∞ to obtain the dimensional surface charge density), which is positive when there is an excess of cations over anions (and thus the electrode matrix is negatively charged); (ii) an equation similar to Eq. (8) for the salt adsorption, w, given by [18,24,54]

$$w = 4\sqrt{c} \sinh^2 \tfrac{1}{4}\Delta\phi_D , \tag{9}$$

which can again be multiplied by $2, \lambda_D^0$, and C_∞, to obtain the dimensional total ion adsorption density; and (iii) a relation between the voltage difference across the charge-free Stern ("inner" or "compact") layer, $\Delta\phi_S$, and the charge density q, as if the Stern and diffuse layers were two capacitors in series [54],

$$q = -\Delta\phi_S / \delta \tag{10}$$

where $\delta = \lambda_S / \lambda_D^0$, where λ_S is an effective thickness of the Stern layer [52].

In recent years, the same Stern boundary condition has also been used extensively in other dynamical situations with time-dependent normal currents, such as capacitive charging of blocking electrodes [24,41,54], fluctuations of ion-conducting biological membranes [57,58], induced-charge electro-osmotic flows [38], and electrofluidic gating [59]. In all of these situations, the dimensionless parameter δ controls the voltage drop across the Stern layer relative to that of the diffuse layer and has two important limiting cases [52]: (i) In the "Gouy-Chapman (GC) limit", $\delta \to 0$, the Stern layer is negligible, and the diffuse layer carries all of the double-layer voltage, as in Gouy's model of the double layer. (ii) In the "Helmholtz (H) limit", $\delta \to \infty$, diffuse charge can be neglected, and the double layer voltage is dropped across the molecular Stern layer, as in the earliest double-layer model proposed by Helmholtz.

The charge transfer rate into the matrix/pore-interface, j_{charge}, relates to the charge density, q, according to

$$\frac{\partial q}{\partial t} = j_{charge} - j_F \tag{11}$$

where j_F is a dimensionless Faradaic reaction rate to be discussed below. Note that here j_F is defined positive when the ion current runs from electrolyte into the electrode (i.e., at the cathode).

Similarly to Eq. (11), the salt adsorption rate, j_{salt}, relates to salt adsorption, w, according to

$$\frac{\partial w}{\partial t} = j_{salt} - j_F . \tag{12}$$

This equation is valid for the situation that at the electrode a monovalent cation reduces to a neutral species, which either diffuses away, or plates out as a metal ion, or is stored in a solid pseudo-capacitor phase. When there are divalent ions involved in the reaction, this equation, and many others above, must be modified. For a purely capacitive process, where $j_F=0$, Eqs. (11) and (12) simplify to equivalent surface conservation laws for planar interfaces [54,55], while for porous electrodes they are in this case similar to Eqs. (8) and (9) of ref. [24].

C. Faradaic reactions in the double layers

To describe the kinetics of the Faradaic reaction, we apply the generalized Frumkin-Butler-Volmer equation, which for a one-electron reaction can be represented in dimensional form as [47-53,60-73]

$$J_F = K_R C_{O,rp} \exp\left(-\tfrac{1}{2}\Delta\phi_S\right) - K_O C_{R,rp} \exp\left(\tfrac{1}{2}\Delta\phi_S\right) \tag{13}$$

where we have assumed the transfer coefficients to be $\alpha_O = \alpha_R = \tfrac{1}{2}$, and where K_R and K_O are kinetic rate constants for the reduction and oxidation reaction (in m/s), respectively, while $C_{O,rp}$ and $C_{R,rp}$ are volumetric concentrations of the reactants/products in the oxidized and reduced state, at the reaction plane (equated with the Stern plane). The ratio K_R/K_O contains thermodynamic information, independent of kinetics. Namely, assuming equilibrium ($J_F=0$), and after implementing the Boltzmann equilibria, $C_{O,rp}=C_{O,\infty}\exp((z-1)\Delta\phi_D)$ and $C_{R,rp}=C_{R,\infty}\exp(z\Delta\phi_D)$ (where z the charge sign of the reduced species), we obtain the Nernst potential, i.e. the equilibrium potential difference across the full interface, $\Delta\phi^{eq} = \ln\left(K_R C_{O,\infty} / K_O C_{R,\infty}\right)$. Thus, at equilibrium, the total voltage drop across the interface, $\Delta\phi$ of Eq. (7), equals the Nernst potential, $\Delta\phi^{eq}$. For non-ideal solutions we can replace concentrations c by activities a, both in Eq. (13) and the Boltzmann equation given above, as in ref. [74], although generally the reaction rates must also be modified to account for non-idealities in the transition state [75]. As reviewed in ref. [71], Eq. (13) extends standard descriptions of Faradaic charge transfer in porous electrodes [1,4,76] where the charge transfer rate depends only on the difference in potential between the conducting matrix and in the pore solution, $\Delta\phi=\phi_1-\phi$ ($\Phi_1-\Phi_2$ in the classical terminology) without considering the structure of the double layer and changes in the local ion concentration at the surface. In the GC limit ($\delta \to 0, \Delta\phi_S = 0$), Eq. (13) reduces to the classical "Chang-Jaffe boundary condition," which postulates standard first-order reaction kinetics at the electrode surface, independent of the local voltage or electric field [77,78,79].

Considering the specific case of a cation reacting to a neutral species ($z=0$) of constant chemical potential (as for the case that the cation plates out of solution), replacing dimensional quantities J, K and C by their dimensionless equivalents j, k and c (by dividing J_F by J^*, K_R and K_O by $2D_e\lambda_D^0/L_e^2$ and C by C_∞), and implementing for the cation the Boltzmann equilibrium, $c_{O,rp}=c\cdot\exp(-\Delta\phi_D)$, we obtain

$$j_F = k_R c \cdot \exp\left(-\Delta\phi_D - \tfrac{1}{2}\Delta\phi_S\right) - j_O \exp\left(\tfrac{1}{2}\Delta\phi_S\right) \tag{14}$$

where additionally $k_O \cdot c_{R,rp}$ has been replaced by the constant j_O. This expression vanishes when the total double-layer voltage $\Delta\phi$ equals the equilibrium Nernst voltage, $\Delta\phi^{eq} = \ln(k_R c / j_O)$, so it is convenient to introduce the dimensionless "surface" or "interfacial" overpotential, $\eta = \Delta\phi - \Delta\phi^{eq}$, and express the dimensionless Faradaic current in the form,

$$j_F = j_O \exp\left(-\frac{q\delta}{2}\right)\left[\exp(-\eta)-1\right]. \tag{15}$$

This formula expresses the generalized Frumkin-Bulter-Volmer model for electrochemical reaction kinetics in the case of symmetric electron transfer ($\alpha=\frac{1}{2}$), and shows that the reaction rate depends not only on the overpotential, but also on the interfacial charge density. An important difference with most prior theories is that the interfacial charge density q is not an arbitrary fitting parameter, but instead is determined uniquely and self-consistently from the local interfacial voltage, normal current, and bulk salt concentration.

In order to gain a simple physical understanding of the kinetic model and to facilitate our mathematical analysis below, it is instructive to again take the Gouy-Chapman (GC) and Helmholtz (H) limits [52,71]:

$$-j_F \sim \begin{cases} j_O\left[1-\exp(-\eta)\right] & \text{Gouy-Chapman (GC) limit} \\ 2\sqrt{j_O k_R c}\,\sinh\left(\dfrac{\eta}{2}\right) & \text{Helmholtz (H) limit} \end{cases} . \tag{16}$$

In the H-limit ($\delta \to \infty$, $q \to 0$), diffuse charge is negligible, and the Faradaic current has the standard Butler-Volmer form for symmetric electron transfer to a quasi-neutral bulk solution in direct molecular contact with the electrode. In the GC limit ($\delta \to 0$, $\Delta\phi_S \to 0$), however, the Frumkin effect of diffuse charge dominates, and the double layer acquires the current-voltage characteristics of a Schottky diode. For large positive overpotentials $\eta \gg 1$, analogous to "reverse bias" of a semiconductor diode, the active cations are strongly expelled from the diffuse part of the double layer by a large excess positive charge on the electrode (relative to the equilibrium charge, which may be positive or negative), thereby eliminating the reduction reaction (cation removal) and leaving only the constant oxidation reaction (cation production). For large negative overpotentials $\eta \ll -1$, analogous to "forward bias" of a diode, the active cations are strongly attracted to the surface and their concentration increases exponentially with (negative) voltage, thereby amplifying the reduction reaction, which dominates the current.

D. Mathematical formulation

Equations (1)-(14) provide a complete description of transient double-layer charging and Faradaic charge-transfer reactions in a porous electrode, given all the stated assumptions. Following ref. [24], it is convenient to reformulate the full set of 14 equations as simply two partial differential equations (PDEs), in this case for the bulk electrolyte concentration c and the double-layer charge density q in the pores, by eliminating the microscopic fluxes j_{charge} and j_{salt} using analytical properties of the GCS model. First, we derive a PDE for the salt concentration c, which expresses mass conservation, by combining Eq. 5 with Eq. 12:

$$\frac{\partial c_{tot}(c,q)}{\partial t} = \frac{\partial^2 c}{\partial x^2} - \epsilon j_F(c,q) \tag{17}$$

where $c_{tot} = c + \int w$ is total mean concentration of ions in the pores, equal to the sum of the bulk salt concentration plus the excess density of ions (of either sign) stored in the double layers per pore volume, which can be expressed as

$$c_{tot}(c,q) = c + \epsilon\left(\sqrt{4c+q^2} - 2\sqrt{c}\right) \tag{18}$$

using a simple formula for $w(c,q)$ in the GCS model [24,29]. Similarly, we can use Eqs. 8, 10 and 14 to express the Faradaic current density as

$$j_F(c,q) = j_O\left[\exp\left(\Delta\phi^{eq} + 2\sinh^{-1}\left(\frac{q}{2\sqrt{c}}\right) + \tfrac{1}{2}q\delta\right) - \exp\left(-\tfrac{1}{2}q\delta\right)\right]$$
$$= k_R c \cdot \exp\left(\frac{q\delta}{2}\right) \cdot \left[-\frac{q}{2\sqrt{c}} + \sqrt{\left(\frac{q}{2\sqrt{c}}\right)^2 + 1}\right]^{-2} - j_O \cdot \exp\left(-\frac{q\delta}{2}\right) \tag{19}$$

Next we obtain a second PDE for the charge density q, which expresses charge conservation, using Eqs. 1, 6 and 11,

$$\int \frac{\partial q}{\partial t} = \frac{\partial}{\partial x}\left(c\frac{\partial \phi(c,q)}{\partial x}\right) - \int j_F(c,q) \tag{20}$$

and finally, we use Eqs. 7, 8, and 10 to eliminate the pore potential

$$\phi(c,q) = \phi_1 + 2\sinh^{-1}\left(\frac{q}{2\sqrt{c}}\right) + q\delta \cdot \tag{21}$$

Substituting Eqs. 18, 19, and 21 into Eqs. 17 and 20, we arrive at two self-contained nonlinear, coupled PDEs for $c(x,t)$ and $q(x,t)$, which constitute the most compact mathematical form of our porous-electrode model including both capacitive charging and Faradaic reactions. Note that, even in the absence of Faradaic reactions (j_F=0), these PDEs are not equivalent to Eqs (15a) and (15b) in Ref. [24], except in the GC-limit, since we have also included the effect of the Stern-layer capacitance. Although this is a significant complication for the mathematical analysis, it allows us to systematically control the effects of diffuse charge on both capacitive charging [54,55] and Faradaic reactions [52,71] by varying the parameter δ.

III. ANALYSIS

A. Dynamical regimes

To illustrate the predictions of the general theory, we analyze the response to a suddenly applied voltage ϕ_1 on the porous electrode (relative to the bulk solution) starting from an equilibrium state at $t=0$. This canonical problem has previously been studied for flat [54,55] and porous [24] blocking electrodes without Faradaic reactions, and it is directly relevant for capacitive energy storage or desalination systems. It also underlies important experimental methods in electrochemistry, such as potentiostatic intermittent titration (stepwise charging of an electrode) and chronoamperometry (transient current analysis following a voltage step). This problem is also convenient to explore the basic physics of the system since it has no imposed scales for time or current, thus leading to a complex multiscale, nonlinear response. In contrast, impedance spectra are modeled by linearizing the transport equations for small voltages (as we do below, only for early times) and seeking a sinusoidal response at a single time scale, selected by the imposed AC frequency [79]. Multiple time scales do arise in the response to a suddenly applied constant current, but the imposed flux boundary condition (in one dimension) constrains the nonlinear dynamics somewhat more strongly than the case of a constant voltage, at least below the diffusion-limited current, since the current must remain uniform across the quasineutral bulk region [72].

There are two fundamental time scales that determine the evolution of the potential and concentration: (i) the small "RC" time scale, $t=O(\epsilon)$, which governs the transient double-layer charge density in Eq. 20, and (ii) the long diffusive time scale $t=O(1)$, which governs the transient bulk salt concentration in Eq. 17. The former corresponds to the "supercapacitor regime" analyzed in ref. [24] for blocking porous electrodes, where the bulk salt concentration remains nearly uniform, $c=1+O(\epsilon)$, and the porous electrode acts like an RC transmission line carrying current through a nearly constant bulk resistance into the double layers. Restoring dimensions, the characteristic charging time scale can be written as

$$\tau_c = \epsilon \frac{L_e^2}{D} = \left(\frac{\lambda_D^0 h_p}{D} \right) \left(\frac{L_e}{h_p} \right)^2 \tag{22}$$

which is the product of RC time for capacitive charging of a characteristic unit pore space [54], whose length is comparable to its thickness, and the square of the number of such pore spaces across the electrode thickness. The crucial difference with Ref. [24], however, is that we consider Faradaic reactions, which contribute charge-transfer resistances in parallel with the double-layer capacitances, as shown in Fig. 2. We also consider the effects of the Stern layer, contributing an extra capacitance and coupling the charge to the reaction rate. As shown below, these effects alter transient response of the porous electrode, including the charging time scale.
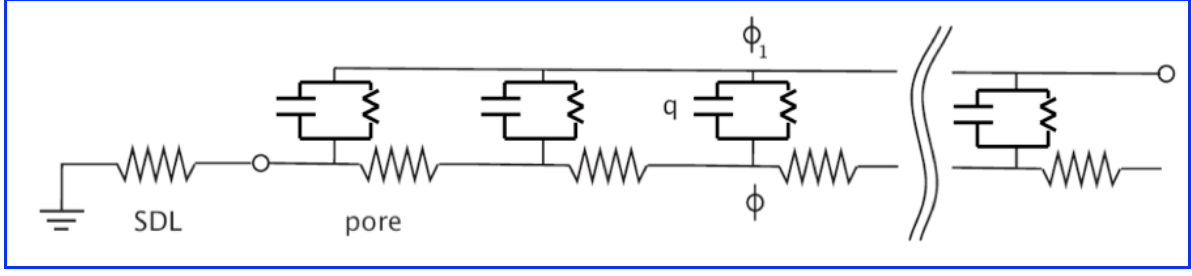
FIG. 2. Equivalent circuit (RC transmission line [80]) for the linear response of the porous electrode in our model including both capacitive charging and Faradaic reactions. The quasi-neutral solution in the pores acts as a series of resistors coupled to the electrode by parallel elements, each of which consists of two parallel elements, namely a charge-transfer resistance and a double layer capacitance (consisting of the diffuse and Stern layer differential capacitances in series [54]).

At the diffusion time scale, L_e^2/D, when $t=O(1)$, the concentration is significantly perturbed, analogous to the "desalination regime" of ref. [24], but with the important difference that a nontrivial steady state is reached, since we assume that the reduced state of the cation, being the product of the Faradaic reaction, is kept at constant chemical potential. This approach neglects for the moment back-diffusion out of the electrode of the (possible neutral) product species, or its intercalation in the solid phase such as for the case of Li-ion batteries and pseudo-capacitors, where for the reduced species only a finite number of sites is available, which (possibly at only very long timescales) leads to the decrease of the Faradaic reaction rate back to zero. As such, we refer to this phase of the dynamics approaching a steady direct current as the "fuel cell" regime. Mathematically, this regime is difficult to describe, even if Eqs. 17 and 20 are linearized for small applied voltages, since the concentration varies together with the charge density. This leads to a linear PDE for the vector (c,q) with 2x2 matrix coefficients, whose solution by Fourier methods is possible, but cumbersome to the point of hindering physical insight. The steady state is more tractable, as we will analyze in section III.C, also allowing for nonlinear response to a large voltage. Transients in the full problem require numerical solution, as described in section IV.

B. Early-time linear response ("supercapacitor regime")

For large overpotentials, the concentration becomes significantly perturbed close to the SDL/electrode interface, as soon as the charging process proceeds into the porous electrode over a significant macroscopic distances. (See section IV.C. below.) For small overpotentials, $|\eta| \ll 1$, and early times $t=O(\epsilon)$, however, the concentration remains close to its initial value, $c \sim 1$, and we can linearize the reaction kinetic equation 15, using

$$j_F \sim -j_O \cdot \exp\left(-\tfrac{1}{2} q^{eq,0}\delta\right) \cdot \eta = -j_{ex}\eta \tag{23}$$

where j_{ex} is the (dimensionless) equilibrium exchange current density. Here, $q^{eq,0}$ is the equilibrium charge density before the voltage is applied (when $c=1$), which satisfies the following transcendental equation

$$2 \cdot \sinh^{-1}\left(\tfrac{1}{2} q^{eq,0}\right) + q^{eq,0}\delta = -\Delta\phi^{eq,0} \tag{24}$$

where $\Delta\phi^{eq,0} = \ln\left(j_O / k_R\right)$ is the equilibrium DL voltage in the initial state with $c=1$. Linearizing the transient charge density around this value, we can use Eqs. 7, 8 and 10 to relate $\partial q / \partial t$ to $\partial \eta / \partial t$ and thus obtain a linear reaction-diffusion-type PDE for the early-time dynamics of the overpotential,

$$\frac{\partial \eta}{\partial \tilde{t}} = \frac{\partial^2 \eta}{\partial x^2} - \mathrm{Da} \cdot \eta . \tag{25}$$

In this equation, we have rescaled the dimensionless time according to

$$\tilde{t} = \left\{ \left[1 + \left(\tfrac{1}{2} q^{eq,0} \right)^2 \right]^{-1} + \delta \right\} \frac{t}{\epsilon} \tag{26}$$

which shows how the RC charging time is affected by the Stern layer in our model by dividing τ_c in Eq. 22 by the factor in braces, effectively putting the Stern-layer capacitance in series with the diffuse-layer capacitance. In Eq. 25, we have also defined an effective Damköhler number

$$\mathrm{Da} = \epsilon\, j_O \cdot \exp\left(-\tfrac{1}{2} q^{eq,0} \delta \right) \tag{27}$$

which measures the importance of Faradaic leakage currents (analogous to a homogeneous reaction consuming the overpotential) compared to capacitive charging of the double layers (analogous to diffusion of the overpotential) in the RC transmission-line equivalent circuit shown in Fig. 2.

Before we solve Eq. 25 for the transient overpotential, let us consider several analytically tractable limits of Eqs. 24, 26 and 27 to better understand the basic scales for linear response. First, suppose that the equilibrium charge density is small, in the sense that the diffuse-layer voltage is much smaller than the thermal voltage. In that case we can linearize Eq. 24 to obtain

$$q^{eq,0} \sim \frac{\Delta\phi^{eq,0}}{1+\delta} \quad \text{and} \quad \mathrm{Da} \sim \epsilon\, k_R^{\frac{\delta}{2(1+\delta)}} j_O^{\frac{2+\delta}{2(1+\delta)}} \qquad \text{(small equilibrium charge)} \tag{28}$$

The first expression shows that the initial equilibrium charge and voltage are related as if the double layer consisted of two capacitors in series, since δ can be interpreted as the ratio of the constant capacitance of the diffuse layer (at low voltage) to that of the Stern layer [52,54]. The second expression shows that parasitic Faradaic currents are small, $\mathrm{Da} = O(\epsilon)$, and do not significantly hinder the diffusive propagation of overpotential in the equivalent RC transmission line. Without any restrictions on the equilibrium charge density, we can also obtain simple formulae in the limiting cases of the GCS double layer model:

$$q^{eq,0} \sim -2 \cdot \sinh\left(\tfrac{1}{2} \Delta\phi^{eq,0} \right) = \sqrt{\frac{j_O}{k_R}} - \sqrt{\frac{k_R}{j_O}} \quad \text{and} \quad \mathrm{Da} \sim \epsilon \cdot j_O \qquad \text{(GC limit)} \tag{29}$$

and

$$q^{eq,0} \sim -\frac{\Delta\phi^{eq,0}}{\delta} \quad \text{and} \quad \mathrm{Da} \sim \epsilon \sqrt{k_R j_O} \qquad \text{(H limit)} \tag{30}$$

The initial equilibrium charge-voltage relation again can be interpreted in terms of capacitors in series, only now either the nonlinear differential capacitance of the diffuse layer in the GC model or the constant capacitance of the Stern layer in the Helmholtz model dominate. From Eqs. 28-31 we conclude that, unless the reactions are very fast, the effective Damköhler number is typically small,

$O(\epsilon)$, for thin double layers, so that the Faradaic reaction contribution can be treated as a small, regular perturbation for early times $\tilde{t} = O(1)$.

The linear response PDE, Eq. 25, can be solved exactly using Laplace or Fourier transforms in infinite space. For our problem with a finite domain and a mixed boundary condition for the SDL,

$$\frac{\partial \eta}{\partial x}\bigg|_{x=0,\tilde{t}} = \mathrm{Bi} \cdot \left(\eta\big|_{x=0} - \eta^0\right), \quad \frac{\partial \eta}{\partial x}\bigg|_{x=1,\tilde{t}} = 0 \quad, \quad \eta\big|_{x,\tilde{t}=0} = 0 \tag{31}$$

we can obtain an exact solution as a generalized Fourier series given by

$$\frac{\phi(x,\tilde{t})}{\eta^0} = 1 - \sum_{n=0}^{\infty} \frac{A_n^2 \lambda_n \sin \lambda_n}{\lambda_n^2 + \mathrm{Da}} \cdot \left(1 - \exp\left(-\left(\lambda_n^2 + \mathrm{Da}\right) \cdot \tilde{t}\right)\right) \cos(\lambda_n \cdot (x-1)) \tag{32}$$

where $\lambda_n \tan \lambda_n = \mathrm{Bi}$, $A_n^2 = \dfrac{4\lambda_n}{2\lambda_n + \sin(2\lambda_n)}$, and $\eta^0 = \phi_1 - \Delta\phi^{eq,0}$ is the initial overpotential, just after the voltage is applied, but prior to any charge relaxation. Here, $\mathrm{Bi} = \dfrac{d_{sdl} L_e}{p L_{sdl}}$ is an effective Biot number measuring the characteristic rate of diffusion in the SDL compared to that of the porous electrode.

Deriving the current requires some care. One cannot use Eq (2) and differentiate the Fourier series (32) term by term because it represents a discontinuous initial condition and thus is not uniformly convergent over the domain ($\tilde{t} \geq 0$, $0 \leq x \leq 1$). On the other hand, the series can be integrated term by term, so we can safely obtain the total current, i_e, by integrating the charge flux in space over the electrode as follows, where the Faradaic current density is linearized using Eq. (23) and the capacitive (displacement) current density is linearized using the initial state double layer capacity C_0:

$$i_e = \int_0^1 j_{\mathrm{charge}} dx = \int_0^1 \left(j_F + \frac{dq}{dt}\right) dx = \int_0^1 \left(-j_{ex}\eta + C_0 \frac{d\phi}{dt}\right) dx$$
$$= -\eta^0 \sum_{n=0}^{\infty} \frac{A_n^2 (\sin \lambda_n)^2}{\lambda_n^2 + \mathrm{Da}} \cdot \left[j_{ex}\left(1 - \exp\left(-\left(\lambda_n^2 + \mathrm{Da}\right) \cdot \tilde{t}\right)\right) + C_0\left(1 + \left(\lambda_n^2 + \mathrm{Da}\right)\exp\left(-\left(\lambda_n^2 + \mathrm{Da}\right) \cdot \tilde{t}\right)\right)\right] \tag{33}$$

where $j_{ex} = j_O \exp(\frac{1}{2}\Delta\phi_S^{eq}) \approx j_O \exp\left(\frac{1}{2}\Delta\phi_S^{eq,0}\right)$ and $C_0 = \dfrac{\epsilon}{\delta + \mathrm{sech}(\frac{1}{2}\Delta\phi_D^{eq,0})}$. In the limit where mass transfer is fast enough within the SDL so as to neglect its concentration gradients ($\mathrm{Bi} = \infty$), Eq. (32) simplifies to

$$\frac{\phi(x,\tilde{t})}{\eta^0} = 1 - \sum_{n=0}^{\infty} \frac{(2n+1)\cdot\pi}{(n+\frac{1}{2})^2 \pi^2 + \mathrm{Da}} \cdot \left(1 - \exp\left(-\left((n+\tfrac{1}{2})^2 \pi^2 + \mathrm{Da}\right)\cdot \tilde{t}\right)\right) \cos((n+\tfrac{1}{2})\cdot\pi\cdot(x-1)). \tag{34}$$

In the same limit $\mathrm{Bi} = \infty$, there is also a simple analytical similarity solution to Eq (25):

$$\eta(x,\tilde{t}) = \eta^0 \cdot \exp(-\mathrm{Da}\cdot\tilde{t})\cdot\mathrm{erfc}\left(\frac{x}{2\sqrt{\tilde{t}}}\right) \text{ and } i_e(\tilde{t}) = -c\frac{\partial\phi(x,\tilde{t})}{\partial x}\bigg|_{x=0,\tilde{t}} = -\eta^0 \cdot \exp(-\mathrm{Da}\cdot\tilde{t})\cdot\sqrt{\frac{1}{\pi\tilde{t}}} \tag{35}$$

which is valid for early times, before the diffusion layer propagates across the electrode, and much more accurate in this regime than any truncation of the Fourier series in Eq. 34.

The physical interpretation of this dynamical regime is that the porous electrode acts like an RC transmission line (Fig. 2). The quasi-neutral pore bulk acts like a chain of resistors, connected in

series to the double layers, described by circuit elements consisting of the double-layer capacitance in parallel with the Faradaic charge transfer resistance. This is a classical model [80], but here we derive systematically it from a general nonlinear formulation and provide analytical formulae for the circuit elements in terms of the microscopic model parameters. In contrast to the case of an ideally polarizable electrode with capacitive charging, where the overpotential satisfies a diffusion equation [24], our PDE for the overpotential, Eq. 25, is of the reaction-diffusion type with an additional decay term to describe local capacitor discharging due to Faradaic reactions.

At longer times, $t=O(1)$, for large applied voltages, the dynamics become highly nonlinear, as the concentration varies together with the electric field and diffuse charge in the pores. The time scale is controlled by the diffusion of salt, in response to ion consumption by Faradaic reactions. Analytical solutions are no longer possible, so for the full problem numerical calculations are required, as described below.
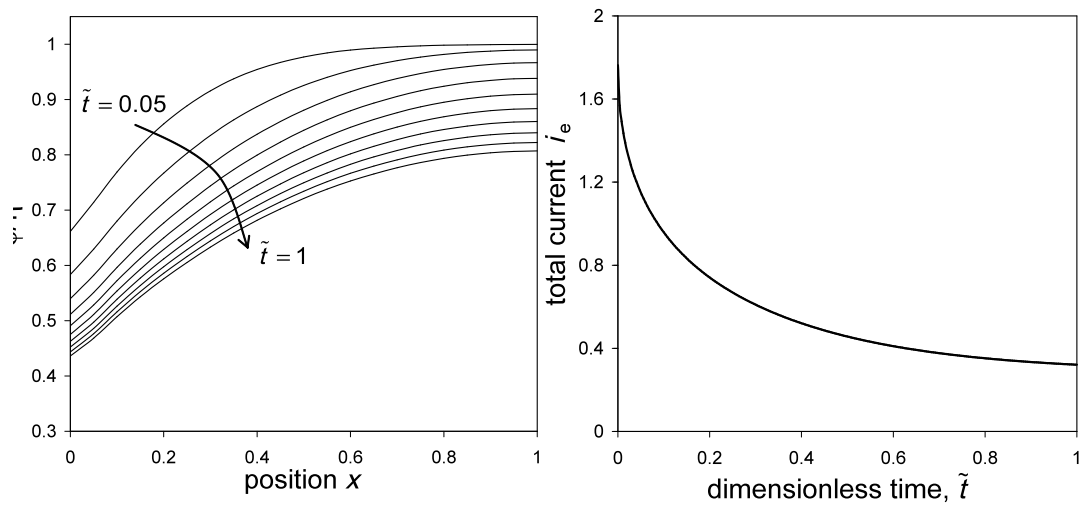

Fig. 3. Early time dynamics in response to a small applied voltage. (a) Evolution of the pore potential as function of position in the electrode as predicted by Eq. (32) for Bi=2 and Da=2 at different values of the dimensionless time $\tilde{t}$. (b) Total current development predicted by Eq. (33) (Bi=2 and Da=2) when a small voltage ($\phi_1 = -1$) is applied.

C. Steady-state nonlinear response ("fuel cell regime")

Once the system reaches steady state, it is again possible to gain analytical insights. First, it is useful to note that all non-reactive ions attain a Boltzmann equilibrium distribution in steady state. In the present calculation these ions are monovalent anions, and thus we have both in the SDL and in the pores of the electrode $\ln(c) = \phi$ at each position. At the solution/electrode-interface we have the classical steady-state expressions

$$c_0 = 1 - i_e / \text{Bi} \; , \quad \phi_0 = \ln(1 - i_e / \text{Bi}) \; , \quad \ln(c_0) = \phi_0 \tag{36}$$

for the salt concentration and potential, as function of the total current i_e. Note that in the electrode the percentage of i_e that is carried by the ions decreases with position, x, starting at 100% at $x=0$ where the ion current $i(x)$ equals i_e, going down to zero at the backside of the electrode. Simultaneously, the

current carried by the electrons in the matrix progressively increases such that i_e is always constant across the electrode.

In the steady-state, the left-hand side of Eq. 5 is zero, and together with setting j_{salt} equal to j_{charge}, which is true because only the reactive cation is being transported in the steady-state, we arrive for the concentration profile inside the electrode at

$$\frac{\partial^2 c}{\partial x^2} = \epsilon j_{charge} \tag{37}$$

which can be solved together with $\ln(c) = \phi$, and Eqs. (7), (8) and (10) to complete the steady-state model. In Eq. (37) we can immediately replace the charging current j_{charge} by j_F of Eq. (14).

For values of $q/(2 \cdot \sqrt{c})$ small, we can derive a single 2nd order differential equation in concentration c, given by

$$\epsilon^{-1} \frac{\partial^2 c}{\partial x^2} = k_R c \cdot \exp\left\{ \frac{1 + \frac{1}{2}\delta\sqrt{c}}{1 + \delta\sqrt{c}} (\ln c - \phi_1) \right\} - j_O \exp\left\{ -\frac{1}{2} \frac{\delta\sqrt{c}}{1 + \delta\sqrt{c}} (\ln c - \phi_1) \right\} \tag{38}$$

In the GC-limit of $\delta = 0$, Eq. (38) can be simplified to

$$\epsilon^{-1} \frac{\partial^2 c}{\partial x^2} = k_R c^2 \exp(-\phi_1) - j_O \tag{39}$$

while in the opposite H-limit of $\delta = \infty$ we obtain

$$\epsilon^{-1} \frac{\partial^2 c}{\partial x^2} = k_R c^{3/2} \exp\left(-\frac{1}{2}\phi_1\right) - j_O c^{-1/2} \exp\left(\frac{1}{2}\phi_1\right). \tag{40}$$

Equations (39) and (40), though derived here from Eq. (38) which is only valid for small values of $q/(2 \cdot \sqrt{c})$, are generally valid, also in the non-linear (large q) regime.

Exact solution for steady linear response

For low values of the initial time overpotential, η^0, and for concentrations c that consequently remain close to unity, Eqs. (39) and (40) can both be simplified to

$$\frac{\partial^2 c}{\partial x^2} = -\mathrm{Da} \cdot \eta^0 \tag{41}$$

with Da defined by Eq. 29 or Eq. 30 for the GC- or H-limit, respectively. This second order ODE has a Dirichlet boundary condition at the inner edge of the electrode, namely at $x=1$ we have $\partial c/\partial x = 0$, while at the edge with the SDL, where $x=0$, we have a Robin mixed boundary condition, given by $\partial c/\partial x = -(1-c) \cdot \mathrm{Bi}$, which follows from combination of Eq. (2) with the steady-state result of Eq. (36). The solution for pore potential ϕ is given by

$$\frac{\phi(x)}{\eta^0} = \frac{1}{2} - \frac{\mathrm{Bi} \cdot \left(\vartheta^{1 - \frac{1}{2}x} + \vartheta^{\frac{1}{2}x}\right)}{2\,\mathrm{Bi} \cdot (1 + \vartheta) - \ln(\vartheta) \cdot (1 - \vartheta)} \tag{42}$$

where $\vartheta = \exp\left(2\sqrt{2\mathrm{Da}}\right)$. Comparison of Eq. (42) with the full numerical results, both in the GC-limit (Eq. (39)) and in the H-limit (Eq. (40)) gave an exact agreement as long as the initial overpotential η^0 was sufficiently low, as shown in Fig. 4.

Note that this result is not equal to the early-time dynamic equation, Eq. (32), when we take the limit of $\tilde{t} \to \infty$, because Eq. (32) will always fail at some point before we approach the steady-state, because in the steady state the gradients in salt concentration, no matter how small, are responsible for half of the current, an effect which is not considered in Eq. (32).

Approximate solutions for steady nonlinear response

Next we derive analytical solutions for both the GC- and H-limits when deep within the electrode concentrations are close enough to zero, e.g., because the electrode potential ϕ_1 is sufficiently negative. For the GC-limit, integrating Eq. (39) once results in

$$\epsilon^{-\frac{1}{2}} \frac{\partial c}{\partial x} = -\sqrt{\tfrac{2}{3} k_R c^3 \exp(-\phi_1) - 2 j_O c + w_2} \tag{43}$$

where the integration constant w_2 follows from the boundary condition of $\partial c/\partial x = 0$ at $x=1$; thus, $w_2 = 2 j_O c_1 - \tfrac{2}{3} k_R c_1^3 \exp(-\phi_1)$ where c_1 denotes $c(x=1)$, i.e., the concentration at the interior edge of the electrode. To integrate Eq. (43) analytically, w_2 must be small as well as the second term on the right-hand side of Eq. (43), $2 j_O c$. In that case, integration of Eq. (43) results in

$$c_{GC}(x) = \left\{ \frac{1}{\sqrt{c_0}} + x \sqrt{\frac{\epsilon k_R \exp(-\phi_1)}{6}} \right\}^{-2} \tag{44}$$

where c_0 denotes $c(x=0)$, i.e., the concentration at the SDL/electrode interface.

For the H-limit, integrating Eq. (40) once results in

$$\epsilon^{-\frac{1}{2}} \frac{\partial c}{\partial x} = -\sqrt{\tfrac{4}{5} k_R c^{\frac{5}{2}} \exp(-\phi_1/2) - 4 j_O c^{\frac{1}{2}} \exp(\phi_1/2) + w_2} \tag{45}$$

where now the integration constant w_2 is given by $w_2 = 4 j_O c_1^{\frac{1}{2}} \exp(\phi_1/2) - \tfrac{4}{5} k_R c_1^{\frac{5}{2}} \exp(-\phi_1/2)$. Again assuming w_2 to be small, as well as the second term in Eq. (45), we now obtain

$$c_H(x) = \left\{ \frac{1}{\sqrt[4]{c_0}} + x \sqrt{\frac{\epsilon k_R \exp(-\phi_1/2)}{20}} \right\}^{-4} . \tag{46}$$

Having solved for concentration $c(x)$, by either of the equations (43)-(46), pore potential $\phi(x)$ follows from $\ln(c) = \phi$, and $w(x)$ and $q(x)$ follow from Eqs. (7)-(10). (Note that in the H-limit, $\delta = \infty$, there is no salt adsorption by the double layers, $w=0$.) The full problem of electrode and SDL requires combination with Eq. (36) for the SDL and an additional relation for the total current i_e to be evaluated at the SDL/electrode interface, which based on $i = -\partial c/\partial x$ follows from Eq. (43) or (45) by multiplying the right-hand side with $-\epsilon^{\frac{1}{2}}$, neglecting the 2nd and 3rd term, and implementing $c=c_0$. The term $x\sqrt{\epsilon k_R}$ in Eqs. (44) and (46) takes the following form with dimensions restored, $X \cdot \sqrt{(K_R/(2 \cdot h_p \cdot D_e))}$, i.e, the steady-state concentration profile depends on the dimensional rate constant K_R, the inverse specific electrode area h_p, and on ion mobility, D_e.

IV. NUMERICAL RESULTS

A. Early time dynamics

In section IV we will give results of numerical and analytical example calculations based on the general theory of section II, and the analytical results derived in section III. We start with an example calculation for the early-time dynamics, showing the voltage in the pores of the electrode after a sudden application of a voltage difference between the metallic (electron-conducting) matrix phase of the electrode (where the potential is ϕ_1) and the electrolyte bulk (outside the SDL). Fig. 3 shows the development of the pore potential profile ϕ and total current i_e in time as function of the dimensionless time $\tilde{t}$ and the effective Biot and Damköhler numbers. Fig. 3 (a) presents general results independent of the value of $\Delta\phi^{eq,0}=\ln(k_R/j_O)$, but let us first discuss the situation that $k_R=j_O$ (i.e., $\Delta\phi^{eq,0}=0$). Then, before and right after application of the potential difference η^0, the potential in the pores remains equal to the voltage in the matrix phase (thus $\phi=\eta^0$), because double layers (DLs) have not yet been formed to sustain any potential difference between matrix and pore. Thus, the total voltage drop between matrix and bulk electrolyte is fully transferred to the SDL. Immediately after applying the voltage difference, near the outer surface of the electrode, counterions start to flow from the SDL into the electrode, to be adsorbed in the nearby DLs, and vice-versa for co-ions, and it is here near the electrode outer edge that DLs first start to be formed with the result that the pore potential moves toward the value in the bulk electrolyte (which we have arbitrarily set to zero). Unless faradaic reactions are zero, equilibrium will never be reached, and thus there will remain a gradient in pore potential. Note that because the analytical equation (32) does not consider the salt concentration in the pores to change in time, it will inevitably break down after some time.

In case $\Delta\phi^{eq,0}\neq0$, then even before perturbing the system (i.e. at equilibrium), the matrix potential ϕ_1 already has an off-set of $\Delta\phi^{eq,0}$ relative to the pore potential ϕ, because DLs are already formed. Shifting the matrix potential further, namely by an amount η^0, leads to the pore potential initially to be shifted by the same amount and leads to the same transport phenomena of ion diffusion and migration into and out of the electrode as when $\Delta\phi^{eq,0}$ would have been zero. The DLs can now be of a higher charge than initially, or likewise can they be of a lower charge or have been charge-reversed, dependent on the signs and magnitudes of $\Delta\phi^{eq,0}$ and η^0.

Total current evolution in Fig. 3 (b) shows that it begins at a large value in response to a suddenly applied large voltage. As time proceeds, the current dramatically drops off to a final steady state current.

B. Steady state

Next, calculation results will be presented for times beyond $O(\epsilon)$, namely of $O(1)$ and beyond. We will describe the profiles across the electrode of concentration c, potential ϕ, charge density, q, and salt adsorption w. In section B we give results for the steady-state, and compare numerical and analytical results, while in section C the transient approach to the steady-state is described.

We will not show in much detail concentrations and potentials in the SDL, for which the behavior is rather straightforward and described e.g. in ref. [24]. Calculation results are based on the following parameter settings: λ_B=0.72 nm, C_∞=10 mM, and thus λ_D^0=3.03 nm. We take a Stern capacity of 1 F/m^2 which translates to λ_S=0.69 nm (when we assume that the dielectric permittivity in the Stern layer is equal to that of water) and thus δ=0.23 will be used in the next two sections (unless we discuss the GC-limit of δ=0 or the H-limit of δ=∞). Furthermore, the porosity equals p=0.5, and the internal surface area is assumed to be a=2·10^7 m^2/m^3, which results in h_p=25 nm, and ϵ =λ_D^0/h_p=0.121 (unless otherwise noted). Finally, we assume L_{sdl}=L_e=100 μm and d_{sdl}=D/D_e=1, which results in Bi=2 (unless otherwise noted). We consider a cathode biased negatively compared to the bulk solution (i.e., ϕ_1<0), where the cations reduce to a neutral species that plates out of solution (i.e., the chemical potential of the product is taken as constant).

First we show results for the H- and GC-limits, which are generally described by Eqs. (39) and (40). For low values of η^0, both equations simplify to Eq. 41, which has Eq. (42) as solution. Fig. 4 presents results for the analytical linear solution, Eq. (42), which is equally valid in the GC- as in the H-limit. Numerical results are presented for the H-limit and we observe how with progressively larger η^0, the profile of pore potential starts to deviate from that predicted by Eq. (42).

Next we remain discussing the GC- and H-limits, using Eqs. (39) and (40), but now go to the other extreme, namely based on taking such negative values of ϕ_1 that concentrations become close to zero at the inner edge of the electrode. For this limit, the analytical results of Eqs. (44) and (46) have been derived. Indeed we observe in Fig. 5 for a length ratio of ϵ=0.5 a nearly perfect fit of the analytical expressions to the full numerical solution of Eq. (38). Reducing the value of ϵ, the salt concentration deep within the electrode increases, and we observe a progressively larger deviation of the analytical expression from the exact result. However, it is interesting to note that the gradient $\partial c/\partial x$ at x=0 (which is proportional to the measurable total current, via Eq. (2) and the anion equilibrium condition c=exp(ϕ)) is still rather well predicted, even at the lowest value of ϵ considered.

Next we show in Fig. 6 results for arbitrary values of δ, thus we are not in either the GC- or H-limit. Fig. 6 shows steady-state profiles for concentration c, electrostatic potential in the pores within the electrode, ϕ, local double layer charge density q and double layer salt adsorption density w as function of position x and applied electrode voltage, ϕ_1. The rate constants are taken equal; thus at equilibrium throughout the electrode the double layer is uncharged and thus also w=0. However, in the steady-state the double layer is highly perturbed from this uncharged state with manifestly non-zero values for q and w. The more negative is the applied voltage ϕ_1 the more the pore solution within the electrode is depleted of salt. Simultaneously, the profiles for charge and salt adsorption, q and w, do not vary in a straightforward manner as function of ϕ_1. The most conspicuous effect is that the profiles of q and w become steeper upon increasing the magnitude of ϕ_1.

Note that the calculation results of Fig. 6 cannot be compared with any of the analytical expressions for the steady-state, because Fig. 6 is based on an intermediate value of δ (namely, δ=0.23) whereas the two analytical expressions are only valid in the GC- and H-limits, and furthermore because salt

concentration in the pore does not remain close to unity and neither goes to zero deep within the electrode.
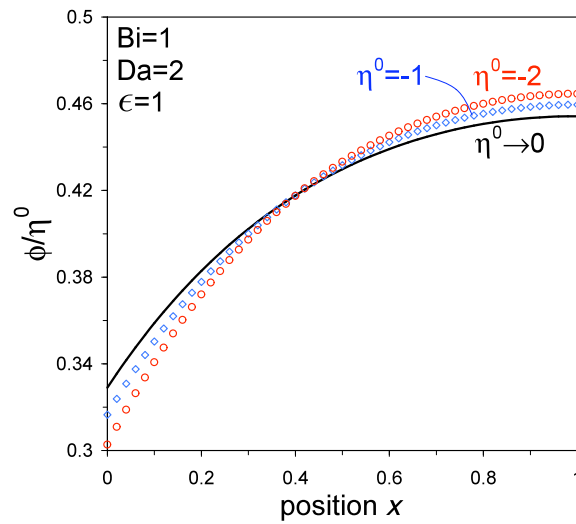

Fig. 4. (Color online). Steady state pore potential ϕ (scaled to η^0) as function of position in the electrode according to Eq. (40) (bullets, H-limit, no further assumptions) and according to Eq. (42) (solid line, both GC- and H-limit, linearized, i.e. pore concentration $c\sim1$). For sufficiently small values of ϕ_1 all steady-state curves will collapse onto the limiting curve (solid line, Eq. (42)).
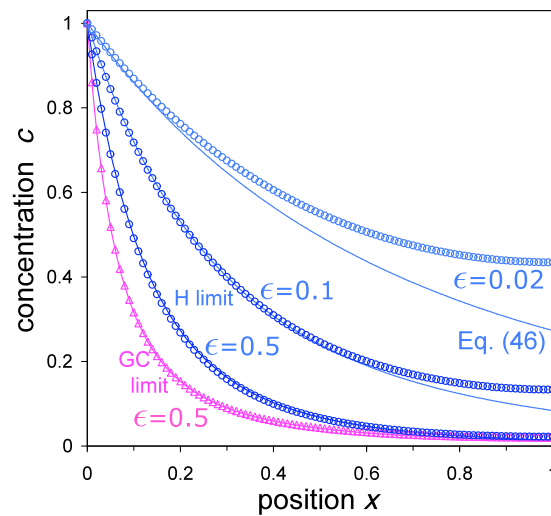
Fig. 5. (Color online). Steady-state profiles of salt concentration in the porous electrode for different values of the ratio ϵ of the Debye length to the mean pore size. Comparison of analytical results (Eqs.(44) and (46)) with full numerical calculations (Eqs. (39) and (40)) in the GC-limit (pink line, triangles) and H-limit (blue lines, bullets). Transport in the stagnant diffusion layer is assumed to be fast (Bi=∞) and other parameter values are η^0=-10; $k_R=j_O$=0.033 (GC-limit) or $k_R=j_O$=1 (H-limit).
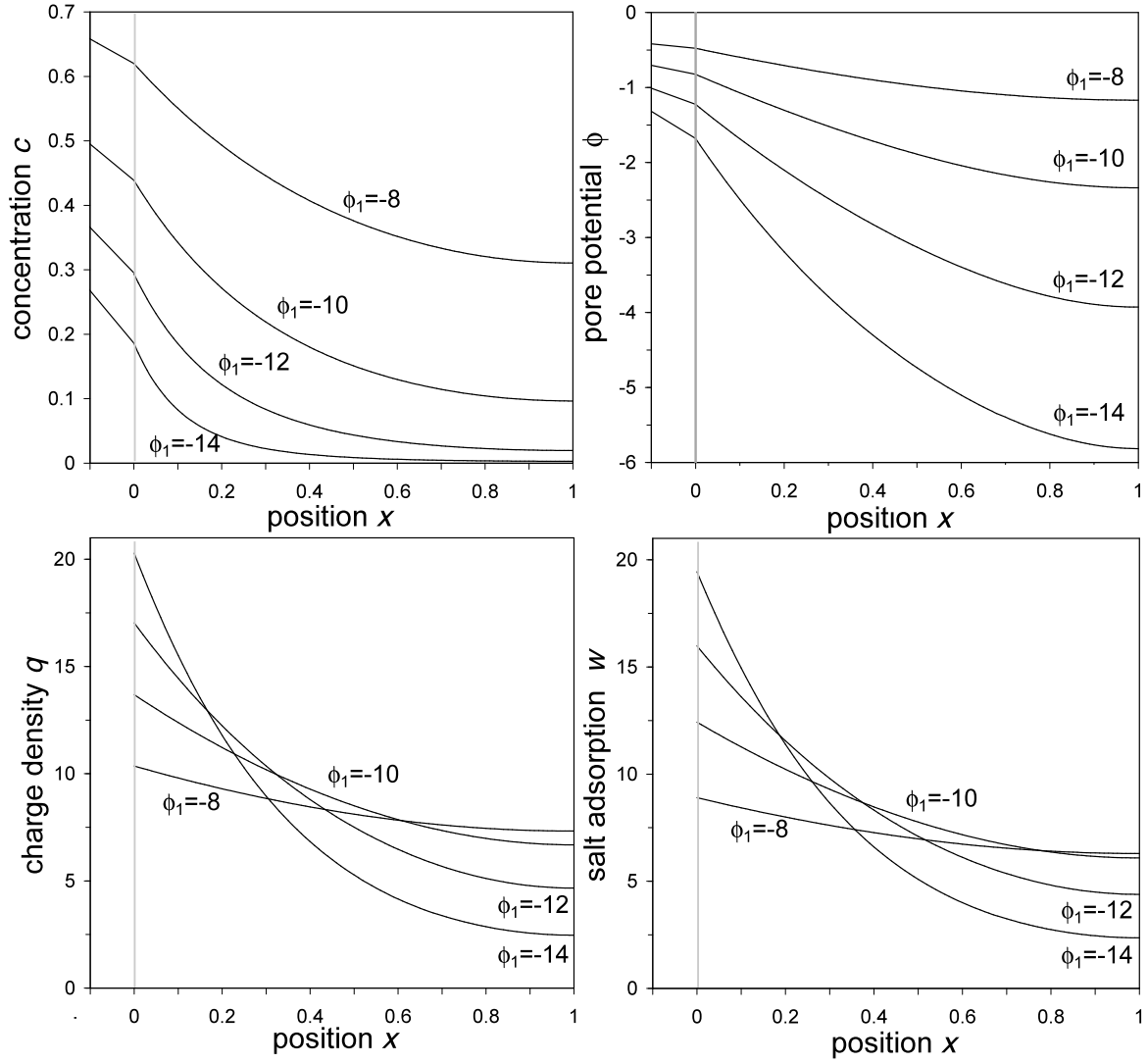
Fig. 6. Numerical results for the steady-state profiles of salt concentration c, pore potential ϕ, diffuse layer charge density q and salt adsorption w in the electrode as function of applied potential ϕ_1 (k_R= j_O=0.033; δ=0.23). For these kinetic rate constants the electrode is uncharged at equilibrium (i.e., $\Delta\phi^0_{eq}$=0).

C. Full numerical results for the dynamics from startup to steady-state

In this final section we return to describing the dynamic evolution of profiles of c, ϕ, q and w toward the steady-state, after a sudden application of an electrode potential ϕ_1. Compared to section A, full numerical results are presented here, and we use parameter settings for which no analytical results seem readily available. In particular, we use high values of the equilibrium double layer potential, $\Delta\phi_{eq}^0$, high values of electrode voltage ϕ_1, and use an intermediate value of δ such that neither the GC- nor the H-limit can be assumed.

Some unexpected, and yet typical, simulation results are presented in Fig. 7 and as a movie online [83]. In this case, we have an equilibrium double layer that is initially negatively charged (excess of anions), which turns positive after applying the voltage, see Fig. 7c. As a consequence of this reversal of sign, we see in Fig. 7a that starting from c=1 first the ion concentration in the pores increases fairly

uniformly across the electrode, by almost 50%, due to the sudden expulsion of ions from the double layer (the opposite process of capacitive desalination, as counterions suddenly become co-ions). Only later does the salt concentration starts to go down significantly to the steady-state profile, where concentrations are on average only 10% of the initial value. Initially this decrease is due to capacitive desalination, or electrostatic attraction of counterions (previously co-ions), and in the last stage it is due to the depletion of active ions by steady Faradaic reactions.

This example clearly illustrates how complex the physics of ion transport and adsorption in a porous electrode can be, and how the dynamical behavior can be very different from the steady state. Panels c and d of Fig. 7 show how charge q starts off at negative values, steadily increases, goes through a maximum before decreasing again and stabilizing at the steady-state profile. Meanwhile, salt adsorption w (which is never negative) first decreases to reach zero at the moment that charge q flips sign (which happens earlier near the outside of the electrode and later deeper within the electrode), after which it increases steadily to a maximum before decreasing again and settling in the steady-state profile.
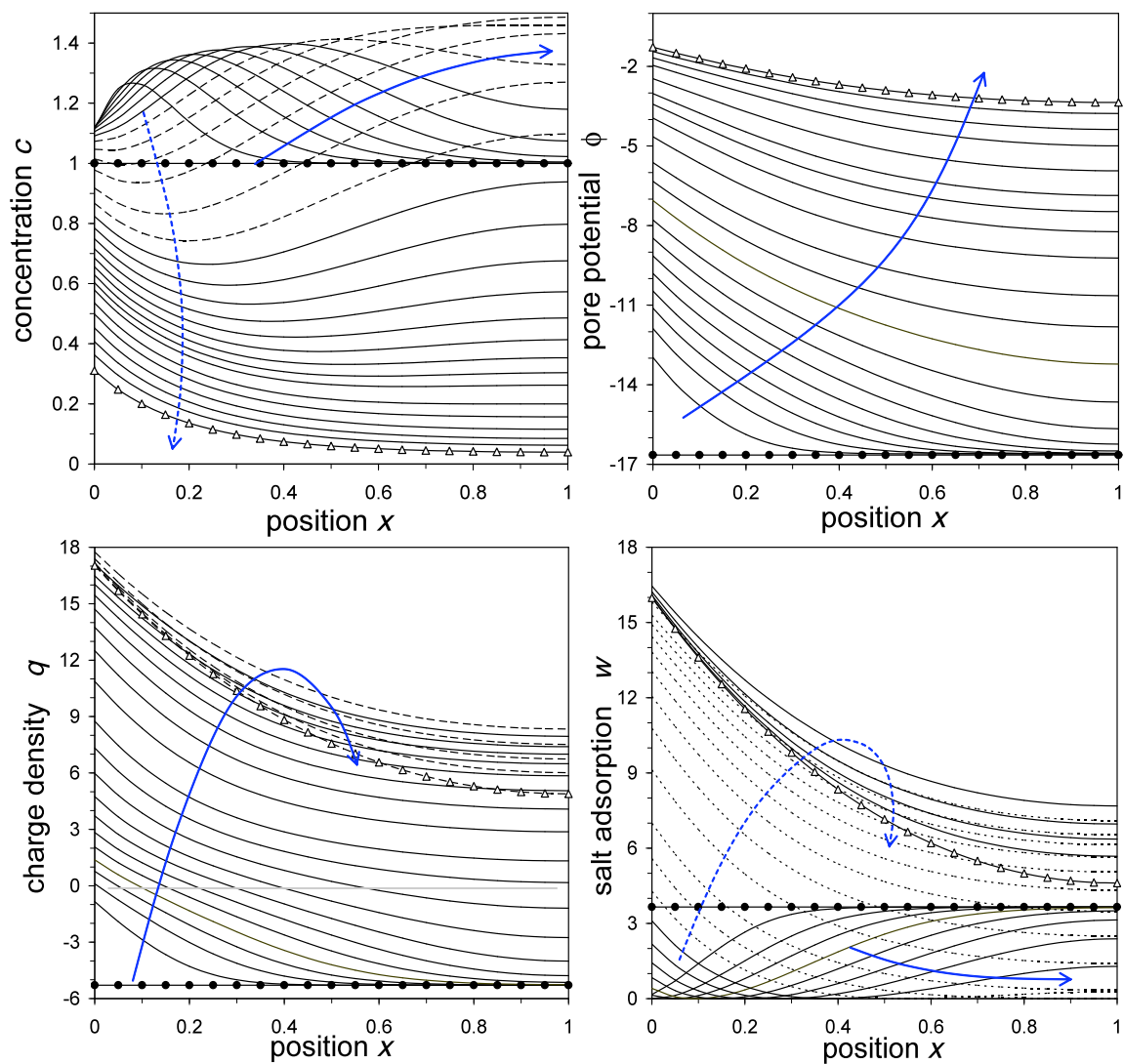
Fig. 7. Numerical results for the profiles of salt concentration c, pore potential ϕ, diffuse layer charge density q and salt adsorption w in the electrode as function of time (direction of arrow, first solid then dashed, and finally solid $0.001<t<3$). Filled circles denote the initial condition and open triangles, the steady-state. The applied voltage (relative to solution) is $\phi_1=-12$, $\delta=0.23$, $k_R=0.033$ and $j_O/k_R=0.01$, i.e., $\Delta\phi^{eq,0}=\ln(k_R/j_O)\sim4.6$. With these settings, the double layers are initially negatively charged, and then eventually become positively charged after the voltage is applied. This sign reversal, coupled to nonlinear dynamics of ion transport at two different time scales (for capacitive and Faradaic charging) leads to the complicated non-monotonic transient seen in the figure. A movie this simulation is available as supporting online material [83].
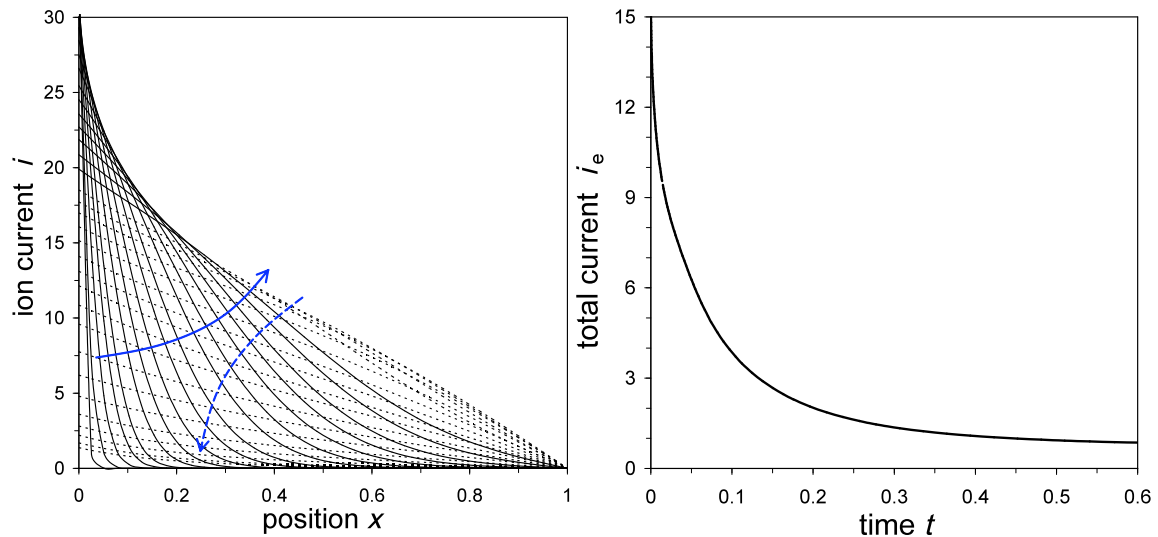

Fig. 8. (a) Ion current profiles in the electrode as function of time. Arrows show the direction of time (solid curves for $0.001<t<0.015$; dashed curves for $0.015<t<0.6$). Ion current at position $x=0$ equals the total current, i_e. (b) Total current i_e versus time t.

For this example, Fig. 8a shows how the ionic current $i(x)$ within the porous electrode gradually decreases with depth and becomes zero at the backside of the electrode. Simultaneously, the current carried by the electrons in the conductive matrix phase progressively increases in this direction so that the total current i_e (which equals the ion current at $x=0$) remains constant at each depth in the electrode. The ionic current initially spreads away from the SDL interface due to diffusive transmission-line propagation of the over-potential. Once the ionic current spreads across the electrode, it relaxes toward the steady state, where Faradaic reactions are continuously fed by the diffusion and electromigration of active species. The total current i_e, plotted as function of time t in Fig. 8b, exhibits a monotonic decay, reminiscent of linear diffusion models that are applied routinely to interpret such data, e.g. in chronopotentiometry for general electrochemical cells [81], or the potentiostatic intermittent titration technique for batteries [82]. This example illustrates how the complex spatiotemporal relaxation of ionic current within a porous electrode (Fig. 8a) can be difficult to discern in the experimentally accessible macroscopic current-voltage response (Fig. 8b), without a detailed mathematical model.

In situations where there is no sign change of the interfacial charge, the dynamics is somewhat simpler. The early stage of the dynamics corresponds to the capacitive desalination process described in Ref. [24], where fast "RC" charging of the double layers is followed by slower depletion of

the salt concentration due to double-layer salt adsorption, which propagates diffusively from the surface into the depth of the porous electrode. Due to Faradaic reactions, however, the present model also captures a later stage of the nonlinear dynamics, where active ions are continuously depleted and fed by diffusion until a steady state profile is reached. An example of this kind of dynamics is shown in Fig. 9 of the Appendix, using the mD model for micropores, rather than the GCS model for macropores.

V. Conclusion

For electrochemical and capacitive cells, we propose a porous electrode-theory that can incorporate any (mathematically explicit) double layer model to describe the dynamics of charge formation and salt storage. In the limit of large pores relative to the Debye length, the Gouy-Chapman-Stern model is a valid approach to describe excess salt and charge storage at the electron conducting matrix/aqueous solution-interfaces within the porous electrode, while in the other limit, of strongly overlapped double layers, a modified Donnan model can be used. Furthermore the theory describes Faradaic charge transfer based on the generalized Frumkin-Butler-Volmer equation which describes the charge transfer rate as a direct function of the local Stern layer potential difference and local ion concentration. Within the macropores of the electrode, and in the outside aqueous solution, ion transport is described by the Nernst-Planck equations combined with local electroneutrality. Both within the GCS-model and the mD-model, charge and salt adsorption in the double layers are analytically related to the diffuse layer (or, Donnan) potential. For both EDL models, the porous electrode theory can be reduced to two coupled nonlinear partial differential equations for the bulk salt concentration and double-layer charge density within the porous electrode. For the GCS-model we have shown that analytical results are possible for small time scales, when the system behaves like an RC transmission line ("supercapacitor regime"), and Faradaic reactions play the role of leakage currents through charge-transfer resistance in parallel with the double layer capacitance. Analytical results are also presented for various limits of the nonlinear response of the system in steady state ("fuel cell regime"). Numerical solutions of the full model are presented for the steady-state as well as for the transient development toward the steady-state of profiles of salt concentration, potential, and surface charge density. These results are directly relevant for capacitive cells used for charge storage (supercapacitors) or salt removal (capacitive deionization). The model can be extended to include volume constraints and other non-idealities for highly concentrated (liquid or solid) solutions, as well as diffusion and volume limitation of reaction products, which arise in applications to batteries and hybrid pseudocapacitors.

REFERENCES

1.   J. Newman and C.W. Tobias, *J. Electrochem. Soc.* **109** 1183 (1962).
2.   A.M. Johnson and J. Newman, *J. Electrochem. Soc.* **118** 510 (1971).

3. J. Newman and W. Tiedemann, *AIChE J.* **21** 25 (1975).

4. J. Newman, *Electrochemical Systems*, Prentice-Hall, (1991). J. Newman and K.E. Thomas-Alyea, *Electrochemical Systems*, Wiley, 3rd Ed. (2004).

5. M.W. Verbrugge and P. Liu, *J. Electrochem. Soc.* **152** D79 (2005).

6. K. Chan and M. Eikerling, *J. Electrochem. Soc.* **158** B18 (2011).

7. B.E. Conway, *Electrochemical supercapacitors*, Kluwer (1999).

8. D. Dunn and J. Newman, *J. Electrochem. Soc.* **147** 820 (2000).

9. Y.M. Vol'fkovich and T.M. Serdyuk, *Russ. J. Electrochem.* **38** 935 (2002).

10. D.B. Robinson, C.-A. Max Wu, and B.W. Jacobs, *J. Electrochem. Soc.* **157** A912 (2010).

11. V. Presser , M. Heon, and Y. Gogotsi, *Adv. Funct. Mat*. **21** 810 (2011).

12. G.W. Murphy and D.D. Caudle, *Electrochimica Acta* **12** 1655 (1967).

13. Y. Oren and A. Soffer, *J. Appl. Electrochem.* **13** 473 (1983).

14. J.C. Farmer, D.V. Fix, G.V. Mack, R.W. Pekala, J.F. Poco, *J. Appl. Electrochem.* **26** 1007 (1996).

15. K.S. Spiegler and Y.M. El-Sayed, *Desalination* **134** 109 (2001).

16. C.J. Gabelich, T.D. Tran, and I.H. Suffet, *Environm. Sci. Techn.* **36** 3010 (2002).

17. T.J. Welgemoed and C.F. Schutte, *Desalination* **183** 327 (2005).

18. P.M. Biesheuvel, *J. Colloid Interface Sci.* **332** 258 (2009).

19. P.M. Biesheuvel, B. van Limpt, and A. van der Wal, *J. Phys. Chem. C*. **113** 5636 (2009).

20. M. Noked, E. Avraham, A. Soffer, and D. Aurbach, *J. Phys. Chem. C* **113** 21319 (2009).

21. Y. Bouhadana, E. Avraham, A. Soffer, and D. Aurbach, *AIChE J.* **56** 779 (2010).

22. R. Zhao, P.M. Biesheuvel, H. Miedema, H. Bruning, and A. van der Wal, *J. Phys. Chem. Lett.*, **1** 205 (2010).

23. H. Li, L. Zou, L. Pan, and Z. Sun, *Env. Sci. & Techn.* **44** 8692 (2010).

24. P.M. Biesheuvel and M.Z. Bazant, *Phys. Rev. E* **81**, 031502 (2010).

25. D. Brogioli, *Phys. Rev. Lett.* **103** 058501 (2009).

26. B.B. Sales, M. Saakes, J.W. Post, C.J.N. Buisman, P.M. Biesheuvel, and H.V.M. Hamelers, *Env. Sci. & Techn.* **44** 5661 (2010).

27. D. Brogioli, R. Zhao, and P.M. Biesheuvel, *Energy & Env. Science* **4** 772 (2011).

28. F. La Mantia, M. Pasta, H.D. Deshazer, B.E. Logan, and Y. Cui, *NanoLetters* **11** xxx (2011). DOI:10.1021/nl200500s

29. N. Boon and R. van Roij, *Mol. Phys*. **109** xx (2011). DOI:10.1080/00268976.2011.554334

30. Y.-T. Kim, K. Tadai and T. Mitani, *J. Mat Chem.* **15** 4914 (2005).

31. S.-W. Lee, N. Yabuuchi, B.M. Gallant, S. Chen, B.-S. Kim, P.T. Hammond, and Y. Shao-Horn, *Nature Nanotech.* **5** 531 (2010).

32. C.-H. Hou, C. Liang, S. Yiacoumi, S. Dai, C. Tsouris, *J. Colloid Interface Sci.* **302**, 54 (2006).

33. M.A. Murad and C. Moyne, *Comput. Geosci.* **12** 47 (2008).

34. A. Revil and N. Linde, *J. Colloid Interface Sci.* **302** 682 (2006).

35. P.M. Biesheuvel, R. Zhao, S. Porada, and A. van der Wal, *J. Colloid Interface Sci.*, submitted (2011).

36. R. Qiao and N.R. Aluru, *J Chem. Phys*. **118** 4692 (2003).

37. L. Joly, C. Ybert, E. Trizac, and L. Bocquet, *Phys. Rev. Lett.* **93** 257805 (2004).

38. M.Z. Bazant, M.S. Kilic, B. Storey, A. Ajdari, *Adv. Colloid Interface Sci.* **152**, 48 (2009).

39. M. Yaniv and A. Soffer, *J. Electrochem. Soc.* **123** 506 (1976).

40. M.D. Levi, S. Sigalov, G. Salitra, R. Elazari, and D. Aurbach, *J. Phys. Chem. Lett.* **2** 120 (2011).

41. M. S. Kilic, M. Z. Bazant, and A. Ajdari, *Phys. Rev. E* **75**, 021502 (2007).

42. P.M. Biesheuvel and M. van Soestbergen, *J. Colloid Interface Sci.* **316**, 490 (2007).

43. P.M. Biesheuvel, *J. Colloid Interface Sci.* **355**, 389 (2011).

44. M.Z. Bazant, B.D. Storey, and A.A. Kornyshev, *Phys. Rev. Lett.* **106** 046102 (2011).

45. A.A. Sonin and R.F. Probstein, *Desalination* **5**, 293 (1968).

46. R.F. Probstein, *Physicochemical Hydrodynamics*, Butterworths (1989).

47. I.B. Sprague and P. Dutta, *Num. Heat Transfer, Part A* **59** 1 (2011).

48. K.J. Vetter, *Electrochemical Kinetics*, Academic Press (1967).

49. V.G. Levich, *Physicochemical Hydrodynamics*, Prentice-Hall (1962).

50. I. Rubinstein, I. Shtilman, *J. Chem. Soc. Faraday Trans. II* **75** (1979) 231.

51. P.M. Biesheuvel and A. van der Wal, *J. Membrane Sci.* **346**, 256 (2010).

52. M.Z. Bazant, K.T. Chu, and B.J. Bayly, *SIAM J. Appl. Math.* **65** 1463 (2005).

53. K.T. Chu, M.Z. Bazant, *SIAM J. Appl. Math.* **65** (2005) 1485.

54. M.Z. Bazant, K. Thornton, and A. Ajdari, *Phys. Rev. E* **70** 021506 (2004).

55. L.H. Olesen, M.Z. Bazant, and H. Bruus, *Phys. Rev. E* **82** 011501 (2010).

56. B. Zaltzman and I. Rubinstein, *J. Fluid Mechanics* **579** 173 (2007).

57. D. Lacoste, G.I. Menon, M.Z. Bazant and J.F. Joanny, *Eur. Phys. J. E* **28**, 243 (2009).

58. F. Ziebert, M.Z. Bazant, and D. Lacoste, *Phys. Rev. E* **81**, 031912 (2010).

59. Z. Jiang and D. Stein, *Langmuir* **26**, 8161 (2010).

60. A. Frumkin, *Z. Physik. Chem.* **164A** 121 (1933).

61. L.I. Antropov, *Kinetics of electrode processes and null points of metals*, Council of Scientific & Industrial Research, New Delhi (1960).

62. R. Parsons, *Adv. Electrochem. Electrochem. Eng.* **1** 1 (1961).

63. E.M. Itskovich, A.A. Kornyshev, M.A. Vorotyntsev, *Physica Status Solidi A* **39** 229 (1977).

64. D. R. Franceschetti and J. R. Macdonald, in *Proc. Third Symposium on Electrode Processes*, Boston, Mass., 7 May 1979; S. Bruckenstein, J.D.E. McIntyre, B. Miller, and E. Yeager, Editors; The Electrochemical Society, 1980 Proceedings Vol. *80-3*; pp. 94-114.

65. G. Horvai, *Electroanalysis* **3** 673 (1991).

66. M. Senda, *Electrochimica Acta* **40** 2993 (1995).

67. A. Bonnefont, F. Argoul, M.Z. Bazant, *J. Electroanal. Chem.* **500** 52 (2001).

68. D.C. Prieve, *Colloids Surfaces A* **250** 67 (2004).

69. A.A. Franco, P. Schott, C. Jallut, and B. Maschke, *Fuel Cells* **2** 99 (2007).

70. P.M. Biesheuvel, A.A. Franco, and M.Z. Bazant, *J. Electrochem. Soc.* **156** B225 (2009).

71. P.M. Biesheuvel, M. van Soestbergen, and M.Z. Bazant, *Electrochimica Acta* **54** 4857 (2009).

72. M. van Soestbergen, P.M. Biesheuvel, M.Z. Bazant, *Phys. Rev. E* **81** 021503 (2010).

73. M. van Soestbergen, *Electrochimica Acta* **55** 1848 (2010).

74. J.W. Tester and M. Modell, *Thermodynamics and Its Applications*, 3rd Ed., Prentice-Hall (1997).

75. P. Bai, D. Cogswell, and M.Z. Bazant, submitted preprint.

76. G. Prentice, *Electrochemical engineering principles*, Prentice-Hall (1991).

77. H. Chang and G. Jaffe, *J. Chem. Phys.* **20** 1071 (1952).

78. J. R. Macdonald, *J. Chem. Phys.* **58**, 4982 (1973).

79. D. R. Franceschetti and J. R. Macdonald, *J. Electroanal. Chem.* **82**, 271 (1977).

80. R. de Levie, *Electrochimica Acta* **8**, 751 (1963).

81. A.J. Bard and L.R. Faulkner, *Electrochemical Methods*, Wiley, 2nd Ed. (2000).

82. R.A. Huggins, *Advanced Batteries*, Springer (2009).

83. See EPAPS Document No. [XXX] for a movie of the simulation in Figure 7. For more information on EPAPS, see http://www.aip.org/pubservs/epaps.html.

Appendix A. Porous electrode theory for the modified Donnan model

In Appendix A we describe the incorporation of the modified Donnan (mD) model for the structure of the electrostatic double layers (EDL) into porous electrode theory [35]. We will neglect Faradaic reactions in this section. The mD-model is valid when the EDLs are strongly overlapped (Debye length much exceeding the pore size), which can be a good approximation for the EDL-structure in the micropores of activated carbon particles. An important difference compared to porous electrode theory using the GCS-model, is that now we must consider two types of porosities, first of all a macroporosity, p_{mA} (corresponding to the porosity p used in the main text), and secondly a microporosity p_{mi} in which the mD-model applies. We define p_{mA} and p_{mi} on the total electrode volume. The micropores are the pores with sizes of no more than a few nm inside the porous (e.g., activated carbon) particles which are the main constituent of the electrode. The macropores (interparticle pore space) are the pathways for ion transport (sizes above 1 μm) in between the particles where the anion and cation concentration are the same. It must be noted that formally the definition of 'macropores' is for pores >50 nm, and micropores for pores <2nm. The bidisperse distribution into micro- and macropores [39] is a useful starting point for the description of many electrode structures, e.g. manufactured from activated carbon particles (typical particle size e.g. 20 μm) with large transport pathways (macropores) in between the particles, and small micropores inside the particles. Ion transport is considered to be limited to the macropores. This distinction in micro- and macroporosity resembles that made in ref. 1, but note that microporosity p_{μ} as defined there is relative to the carbon particle volume, not the total electrode volume.

The mD-model is based on chemical equilibrium for each of the ion types between the macropores and the micropores [33,34], resulting in a Boltzmann-distribution, extended to include a non-electrostatic attraction of the ion into the micropore, μ_{att}. This attraction-term will generally be different for all ions. In the theory below, however, we will set the value of μ_{att} equal for the anion and cation. In the Donnan-approach, there is a mean, common, electrostatic potential in the micropores, the difference with the potential in the macropores, ϕ, given by the Donnan potential, $\Delta\phi_D$. The concentration of ion i in the micropore volume is given by

$$c_{i,mi} = c \cdot \exp\left(-z_i \cdot \Delta\phi_D + \mu_{att}\right) \tag{A-1}$$

where c is the dimensionless macropore salt concentration (similar to the main text defined by $c=C/C_\infty$), and where $z_i=+1$ for the cation and $z_i=-1$ for the anion. The micropore dimensionless charge density $q_{mi} = \frac{1}{2}\left(c_{cation,mi} - c_{anion,mi}\right)$ relates to the Stern layer potential drop across an inner or 'compact' layer separating the ion-containing electrolyte volume in the micropores, from the electron-conducting matrix, according to

$$q_{mi} = -e^{\mu_{att}} c \sinh\Delta\phi_D = -\Delta\phi_S / \delta_{mD} .\qquad\qquad(A\text{-}2)$$

where the dimensionless ratio δ_{mD} is analogous to δ in Eq. 10 in the main text, with δ_{mD} given by

$\delta_{mD} = \dfrac{2FC_\infty h_{p,mi}}{V_T C_{St}}$. In Eq. (A-2), $h_{p,mi}$ is the volume/area ratio for the micropores, F is Faraday's constant and C_{St} the Stern layer capacity. As Eq. (A-2) shows, in the mD-model $C_{St}/h_{p,mi}$ is a lumped parameter, namely the 'volumetric Stern capacity', i.e., the mD-model does not explicitly consider a volume/area ratio. Furthermore we define a dimensionless salt adsorption $w_{mi} = \frac{1}{2}\left(c_{anion,mi} + c_{anion,mi}\right) = ce^{\mu_{att}}\cosh\Delta\phi_D$.

Following section II.D, Eq. 17, we set up a ion balance for the total ion concentration (summing over both porosities) and making use of $w_{mi}^2 = q_{mi}^2 + \left(ce^{\mu_{att}}\right)^2$ we arrive for the mD-model at

$$\frac{\partial}{\partial t}\left(p_{mA}\cdot c + p_{mi}\cdot\sqrt{q_{mi}^2 + \left(ce^{\mu_{att}}\right)^2}\right) = p_{mA}\frac{\partial^2 c}{\partial x^2} .\qquad\qquad(A\text{-}3)$$

Likewise, in the mD-model the local charge balance of Eq. 21 is given by

$$p_{mi}\frac{\partial q_{mi}}{\partial t} = p_{mA}\frac{\partial}{\partial x}\left(c\frac{\partial\phi}{\partial x}\right) .\qquad\qquad(A\text{-}4)$$

Eqs. (A-1)-(A-4) give a full description of porous electrode transport in combination with the mD-model, together with Eq. 7 which relates pore and matrix potentials (ϕ and ϕ_1) to $\Delta\phi_D$ and $\Delta\phi_S$.

In Fig. 9 we give an example calculation using $p_{mi}=p_{mA}=0.30$, $\mu_{att}=1.5$ kT, and $\delta_{mD}=1.25$ (based on $C_{St}/h_{p,mi}=0.12$ GF/m^3 and $C_\infty=20$ mM, all numbers from ref. [35]). We take equal diffusivities in the macropores and in the SDL ($d_{sdl}=1$) and also set the thickness equal, $L_{sdl}=L_e$. We show in Fig. A-1 the macropore salt concentration after a sudden application of an electrode (matrix) voltage of $\phi_1=20$ (relative to the bulk solution outside the SDL; note that the sign of the applied voltage makes no difference in this calculation), similar to Fig. 4b in ref. [24], but now using the mD-model and including the Stern layer (which was not considered in the calculations in ref. [24]) and going to deeper desalination within the electrode. First a local minimum develops in the salt concentration near the outer edge, which flattens out when the minimum in salt concentration is reached around $t\sim0.8$ ($c_{min}\sim0.001$), after which concentrations slowly increase again (grey curves) to go back finally to $c=1$ (final curve shown is for time $t\sim10$).
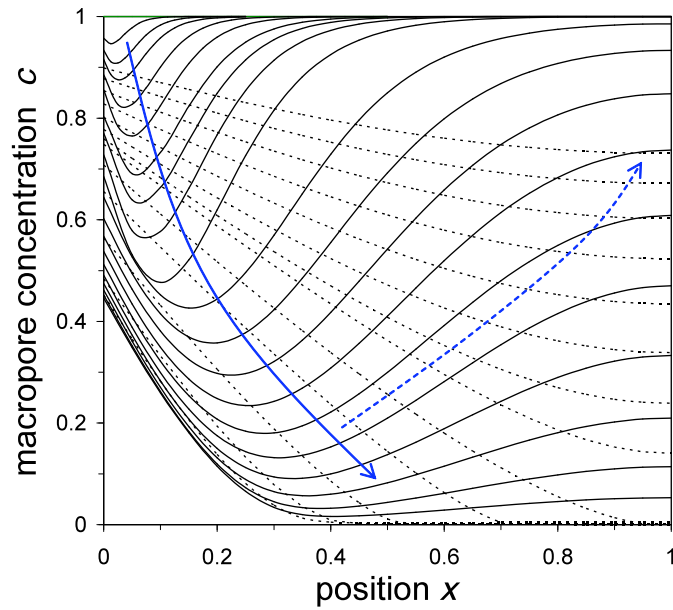
Fig. 9. Macropore concentration profiles within the electrode as function of time using the modified Donnan model. Starting at concentrations c=1, after applying a voltage of ϕ_1=20, first a local dip in concentration develops which flattens out (solid lines and arrow) while concentrations deep within the electrode reach a minimum (t~0.8), after which the salt concentration in the macropores slowly increases again (dashed lines and arrow).